General Disclaimer

One or more of the Following Statements may affect this Document

- This document has been reproduced from the best copy furnished by the organizational source. It is being released in the interest of making available as much information as possible.

- This document may contain data, which exceeds the sheet parameters. It was furnished in this condition by the organizational source and is the best copy available.

- This document may contain tone-on-tone or color graphs, charts and/or pictures, which have been reproduced in black and white.

- This document is paginated as submitted by the original source.

- Portions of this document are not fully legible due to the historical nature of some of the material. However, it is the best reproduction available from the original submission.

SEMIANNUAL REPORT FOR

Grant No. NAG 1-500

SEMICONDUCTOR SUPERLATTICE PHOTODETECTORS

January, 1985 to June 30, 1985

Submitted to

Dr. Charles E. Byvik

FED M/S 283
National Aeronautics and Space Administration
Langley Research Center, Hampton, VA 23665

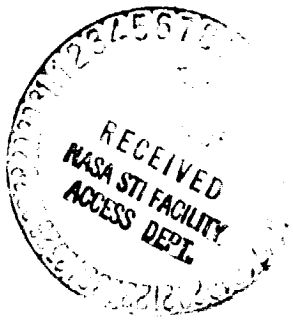

Prepared by

S. L. Chuang

Department of Electrical and Computer Engineering
University of Illinois at Urbana-Champaing
Urbana, IL 61801

and

K. Hess, J. J. Coleman, and J. P. Leburton

Department of Electrical and Computer Engineering
and
Coordinated Science Laboratory
University of Illinois at Urbana-Champaign
Urbana, IL 61801

SEMIANNUAL REPORT FOR

Grant No. NAG 1-500

SEMICONDUCTOR SUPERLATTICE PHOTODETECTORS

January, 1985 to June 30, 1985

Submitted to

Dr. Charles E. Byvik

FED M/S 283
National Aeronautics and Space Administration
Langley Research Center, Hampton, VA 23665

Prepared by

S. L. Chuang

Department of Electrical and Computer Engineering
University of Illinois at Urbana-Champaing
Urbana, IL 61801

and

K. Hess, J. J. Coleman, and J. P. Leburton

Department of Electrical and Computer Engineering
and
Coordinated Science Laboratory
University of Illinois at Urbana-Champaign
Urbana, IL 61801

TABLE OF CONTENTS

I. INTRODUCTION

The research grant NAG 1-500 entitled "Semiconductor Superlattice Photodetectors" was awarded to the University of Illinois by NASA-Langley Research Center on June 27, 1984. Dr. Charles E. Byvik of NASA is the Technical Officer, and Mr. John F. Royall is the Grants Officer. The total amount of funds received by the University is $62,801 to cover the period from July 1, 1984 to June 30, 1985.

This report is the second semiannual report.

1. Period

   January 1, 1985 to June 30, 1985.

2. Reporting Date

   July 5, 1985

3. Technical Personnel

   S. L. Chuang: Assistant Professor of Electrical and Computer Engineering and TRW Assistant Professor of Electrical and Computer Engineering

   J. J. Coleman: Professor of Electrical and Computer Engineering and Research Professor of Coordinated Science Laboratory

   K. Hess: Professor of Electrical and Computer Engineering and Research Professor of Coordinated Science Laboratory

   J. P. Leburton: Assistant Professor of Electrical and Computer Engineering and Research Assistant Professor of Coordinated Science Laboratory

   Peter J. Mares: Research Assistant of Electrical and Computer Engineering

II. TECHNICAL PROGRESS

We studied two novel types of superlattice photodetectors: (1) a superlattice photomultiplier and (2) a photodetector based on the real-space transfer mechanism. A summary of the results is given in this report.

1. Superlattice photomultiplier

The configuration of the device is shown in Figure 1. The optically generated electrons are accelerated by the applied electric field and "impact ionize" the electrons confined in the quantum wells. Thus it works as a solid state photomultiplier. An outline of the theoretical formulation has been given in our first Semiannual Report [1] and a detailed discussion will be presented in a future publication [2].

We have calculated numerically the ionization rate in the computer. An upper limit of the ionization rate $\langle\frac{1}{\tau}\rangle_u$ is obtained easily by ignoring the fact that the final momenta of the electrons need to be larger than a threshold value. The exact numerical integration for the ionization rate $\langle\frac{1}{\tau}\rangle$ takes into account the threshold value for the momenta and needs more computer time. Both results have been calculated and shown in Figures 2 to 7 as functions of the incident electron energy E_0. The necessary material parameters used here are taken from refs. 3 and 4.

The average ionization rate $\langle\frac{1}{\tau}\rangle$ involves the integration over the incident energy E_0 and the distribution function. The function $\langle\frac{1}{\tau(E_0)}\rangle$ multiplied by $\exp(-E_0/k_BT_e)$ is represented by the dashed line in Figure 2. One sees that the main contribution arises from energies between the threshold value and 0.6 eV where $\langle\frac{1}{\tau(E_0)}\rangle \exp(-E_0/k_BT_e)$ has decreased by about two orders of magnitude from its peak value. If the electron temperature T_e is

increased, the slope of the dashed line ($-1/k_B T_e$) will be flatter, and the average ionization rate will increase.

The upper limit of the impact ionization rate as a function of the energy E_0 is shown as the dotted line in Figure 2. This curve is much easier and faster to evaluate since analytical expressions could be obtained with approximations. They also can serve as a means of checking the numerical accuracy of the exact numerical integrations.

In Figure 3, we increase the doping concentration in the quantum-well region to 1.0×10^{18} cm^{-3}. Since there are more electrons in the quantum well than those for the previous case in Figure 2, the ionization rate is larger than that in Figure 2. In Figure 4, the width L_z of the quantum well is decreased to 360Å. The other parameters are the same as those in Figure 2. The impact ionization starts at lower threshold. This is because the momentum of the electron in the quantum-well region has the component π/L_z which is increased. It becomes easier to be ionized. In Figure 5, the mol. fraction x of AℓAs in the $Aℓ_xGa_{1-x}As$ region is decreased to 0.20. The band edge discontinuity ΔE_c is then smaller. Again the impact ionization rate increases and starts at E_0 equal to zero. Thus, ΔE_c provides enough momentum for impact ionization immediately. Note that we have taken into account the difference of the effective masses in different regions. The energy due to the momentum of the electron in the direction parallel to the interface provides part of the energy required for ionization.

In Figures 6 and 7, we reduce the temperature to T = 77°K, T_e = 385°K. We have x = 0.2 for Figure 6 and x = 0.25 for Figure 7. The dashed line decreases much faster compared with the previous cases with T_e = 1500°K as expected.

In Figure 8, the average ionization rate $\langle \frac{1}{\tau} \rangle$ is shown as the solid line as a function of the doping concentration. The upper limit $\langle \frac{1}{\tau} \rangle_u$ is shown as the dotted line. It is clear that the average transition rate is increased generally because more electrons reside in the quantum-well available for ionization. More calculations on various quantum-well sizes are necessary since the quantization effect will be more important if the well size is smaller than 400Å.

2. Photodetector based on the real-space transfer mechanism

Photodetectors play vital roles in optical communication, laser range finding, active laser imaging and picosecond light pulse measurement [5-8]. Today, photodetectors operate over a wide range of wavelengths. In our case, the detection wavelength of interest lies in the micron range (2 to 12 microns) which corresponds to a conduction band edge discontinuity ΔE_c:

$$\Delta E_c \cong 85\% * \Delta E_G^{\Gamma} = 1.06\ x \qquad (0 < x \leq 0.45)$$

where x is the mole fraction of the AℓAs in the $A\ell_xGa_{1-x}As$ region, and ΔE_G^{Γ} is the energy gap difference between the two regions [3]. Through bandgap engineering, i.e., proper selection of the $A\ell_xGa_{1-x}As$ alloy composition, the photodetector may be tailored to achieve desired wavelengths. For example, for an atomic fraction of $x = 0.1$, $\Delta E_c = 0.106$ eV, the corresponding wavelength for absorption is approximately 12 microns. If $x = 0.45$, $\Delta E_c = 0.477$ eV, the absorption wavelength is 2.6 microns.

A photodetector based on the real-space transfer mechanism is shown in Figure 9 [9,10]. Hess et al. [11,12] have investigated this real-space transfer mechanism for its negative differential conductivity and its fast

switching and storage properties. We have examined its optical applications. In particular, the optical free carrier absorption coefficient, which is related to the gain, the fast response time, and the detectivity of the heterostructure photodetector, has been investigated.

The real-space transfer mechanism is the key to the operation of this photodetector. The basic structure of this device consists of a series of alternating GaAs and $A\ell_xGa_{1-x}As$ multilayers (Fig. 9). However, other lattice-matched materials having dissimilar bandgap energies and electron mobilities may be used. The $A\ell_xGa_{1-x}As$ is doped n-type. Before the photodetector is exposed to an optical signal, the electrons from the $A\ell_xGa_{1-x}As$ layers spill into and reside in the well regions. When there is an applied field parallel to the $A\ell_xGa_{1-x}As$ - GaAs interface, they conduct essentially in the GaAs quantum-well regions. When separated from their parent donors by more than 200Å, these electrons experience strongly reduced impurity scattering [9,13,14]. As a result of this and due to the characteristics of GaAs, these electrons experience very high mobilities. On the other hand, the mobility is low in the $A\ell_xGa_{1-x}As$ layers due to the high doping concentration. When the device is optically illuminated with photons whose energies are sufficient to excite the electrons out of the GaAs quantum well, the majority of the thermionically emitted electrons will then conduct in the low mobility $A\ell_xGa_{1-x}As$ layers. This will cause a change in the conductivity and therefore a change in the current density to occur as the electrons depart the GaAs layers. This change in current is a consequence of the decreased population of electrons in the GaAs layers and the lower mobility of the electrons in the $A\ell_xGa_{1-x}As$ layers. Hence, a distinct optical signal may be detected.

The optical absorption coefficient was calculated from the free carrier absorption. In this research, we applied a second-order time-dependent perturbation theory since a phonon is considered in the photon absorption process [15]. Intra-subband optical transitions in which the carriers either (1) absorb a photon and then emit or absorb a phonon or (2) emit a photon and then emit or absorb a phonon, account for the absorption of electromagnetic radiation. The optical frequencies Ω are lower than those which give rise to direct interband transitions in semiconductors, i.e., $h\Omega < E_g$ where E_g is the bandgap of the semiconductor. Since III-V compound semiconducting materials and the $Al_xGa_{1-x}As$-GaAs system in particular are weakly ionic, polar optical phonon scattering plays a part in determining the free carrier absorption. Consequently, we have calculated the free carrier absorption for the case when polar optical phonon scattering of the free carriers is dominant. For the interaction with the radiation field, we considered the case where the radiation field is polarized in the plane of the layer. For the scattering of the carriers by polar optical phonons, we considered only the interaction of longitudinal optical phonons with the carriers. The interaction between the carriers and the transverse optical phonons and the screening of the interaction by the free carriers are assumed to be negligible. We considered the case where the confined carriers are coupled to bulk LO phonons and assumed that the bulk phonons are totally unaffected by the existing quasi-two-dimensional structure. Consequently, the electron-polar optical phonon coupling may be obtained from Frohlich's model.

The computation of the free carrier absorption from an initial bound state where the electron is in the quantum well to a final free state where the electron is out of the well (see Figure 10) was performed in two parts.

First, we considered the absorption in which the intermediate step was a free state, as shown in Figure 10a. Next, as shown in Figure 10b, we considered the absorption for the case of an intermediate bound state. The total absorption coefficient is the sum of the absorption coefficients of each of the respective parts. Having formulated the absorption coefficient, we performed the calculations

$$\alpha_T = \alpha_A^a + \alpha_A^e - \alpha_E^a - \alpha_E^e$$

where α_T is the total absorption coefficient. The subscripts A and E refer to the absorption and emission of photons, respectively. Similarly, the superscripts a and e refer to the absorption and emission of phonons, respectively. For example, α_A^a is due to the absorption of both a photon and a phonon, and α_A^e is due to the absorption of a photon and the emission of a phonon, etc.

We have completed the sophisticated theoretical formulations. Studies, which will include the numerical calculations and the transition without the phonons, will be done in the future.

REFERENCES

[1] S. L. Chuang, K. Hess, J. J. Coleman and J. P. Leburton, Semiannual report for July 1, 1984 to December 31, 1984, Semiconductor Superlattice Photodetectors, January 5, 1985.

[2] S. L. Chuang and K. Hess, "Impact ionization across the band edge discontinuity of quantum well heterostructures", (in preparation).

[3] H. C. Casey, Jr., and M. B. Panish, Heterostructure Lasers, Part A: Fundamental Principles, Academic Press, Inc., New York, 1978.

[4] J. S. Blakemore, J. Appl. Phys., 53, R123 (1982).

[5] D. Botez and G. J. Herskowitz, "Components for optical communications systems: a review," Proc. IEEE, 68, 689 (1980).

[6] J. Conradi, F. P. Kapron and J. C. Dyment, "Fiber-optical transmission between 0.8 and 1.4 μm," IEEE Trans. Electron Devices, ED-25, 180 (1978).

[7] T. P. Lee, C. A. Burrus, Jr., and A. G. Dentai, "InGaAs/InP p-i-n photodiodes for lightwave communications at the 0.95 - 1.65 μm wavelength," IEEE J. Quantum Electron; QE-17, 232 (1981).

[8] U. Koren, et al., "Recent developments in monolithic integration of InGaAsP/InP optoelectronic devices," IEEE J. Quantum Electron., QE-18, 1653 (1982).

[9] H. Shichijo, K. Hess and B. G. Streetman, "Real space electron transfer by thermionic emission in GaAs-$Al_xGa_{1-x}As$ heterostructures: analytical model for large layer widths," Solid State Electron., vol. 23, pp. 817-822, 1980.

[10] K. Hess, B. G. Streetman and H. Morkoc, "Negative resistance heterojunction devices", U.S. Patent No. 4257055, March 1981.

[11] K. Hess, H. Morkoc, H. Shichijo, and B. G. Streetman, "Negative differential resistance through real-space electron transfer," Appl. Phys. Lett., vol. 35, pp. 469-471, 1979.

[12] M. Keever, K. Hess, and M. Ludowise, "Fast switching and storage in GaAs-$Al_xGa_{1-x}AS$ heterojunction layers," IEEE Electron Devices Lett., vol. EDL-3, pp. 297-300, 1982.

[13] R. Dingle, H. L. Störmer, A. C. Gossard and W. Weigmann, Appl. Phys. Lett. 33, 665 (1978); L. Esaki and R. Tsu, IBM Research Report No. RC-2418 (1969).

[14] K. Hess, Appl. Phys. Lett., vol. 35, 484 (1979).

[15] Halina Adamiska and Harold W. Spector, "Free carrier absorption in quantum well structure for polar optical phonon scattering", J. Appl. Phys., vol. 56, No. 4, 15 August 1984, pp. 1123-1127.

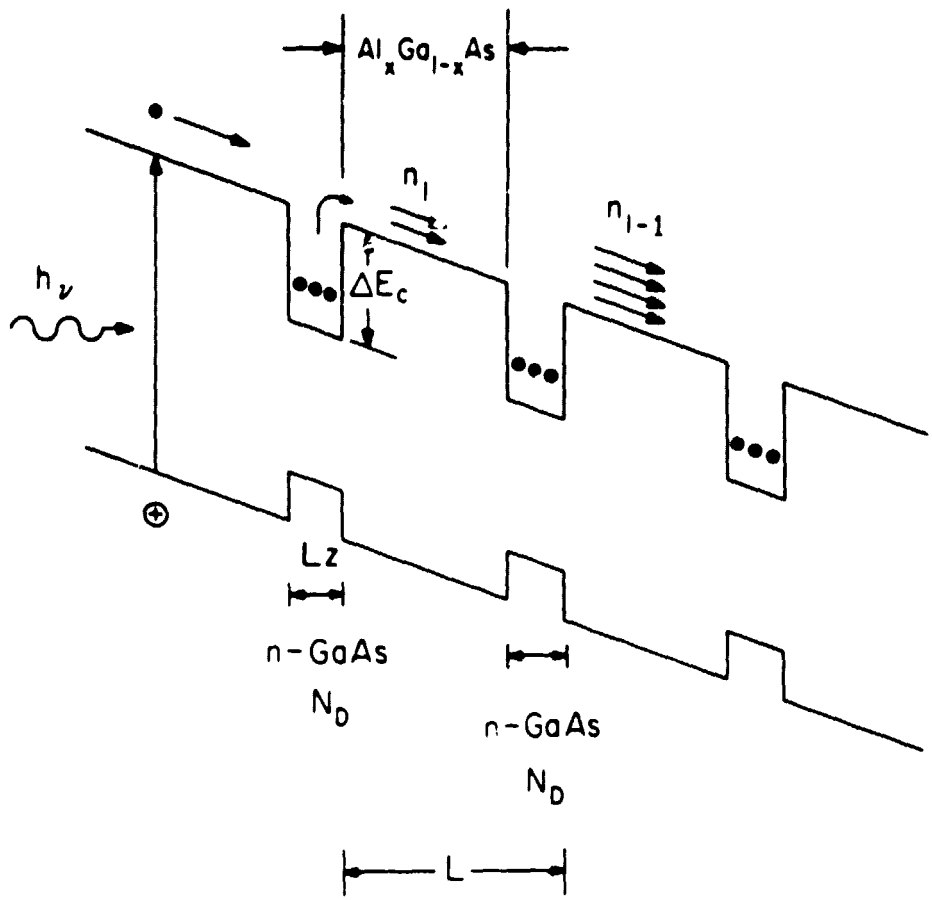

Figure 1. Geometrical configuration of the impact ionization across the band-edge discontinuity in a quantum-well heterostructure.

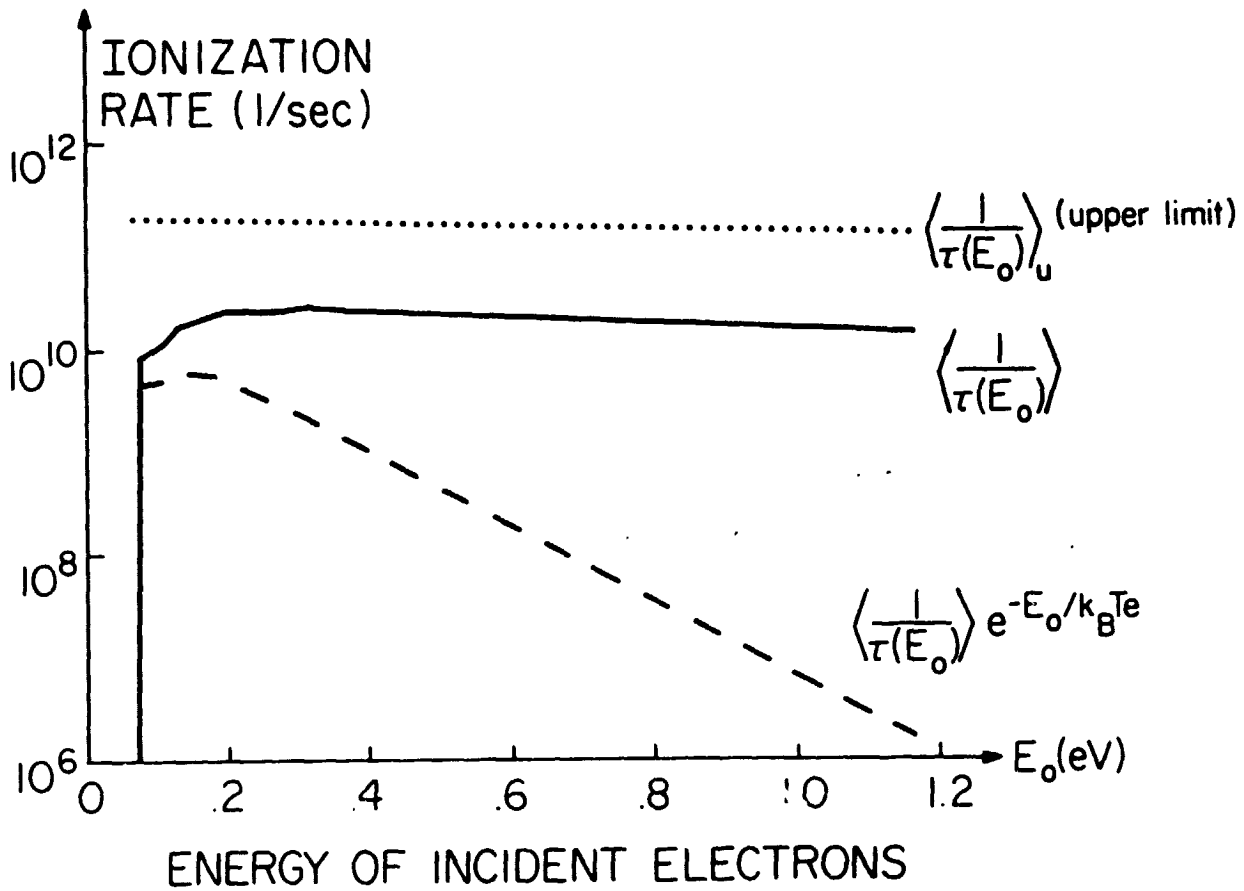

Figure 2. The impact ionization rate $\left\langle \frac{1}{\tau(E_0)} \right\rangle$ as a function of the incident hot electron energy E_0 ——— solid curve. The dashed curve, which is the ionization rate multiplied by $\exp(-E_0/k_B T_e)$, illustrates the trend of the integrand to obtain the average ionization rate. The dotted line is the upper limit of the impact ionization rate. The parameters used are $N_D = 1.0 \times 10^{17}$ cm^{-3}, x = 0.25, L_z = 400Å, L = 1200Å, T = 300°K, T_e = 1500°K, m* = 0.073 m_0, m_0^* = 0.0825 m_0.

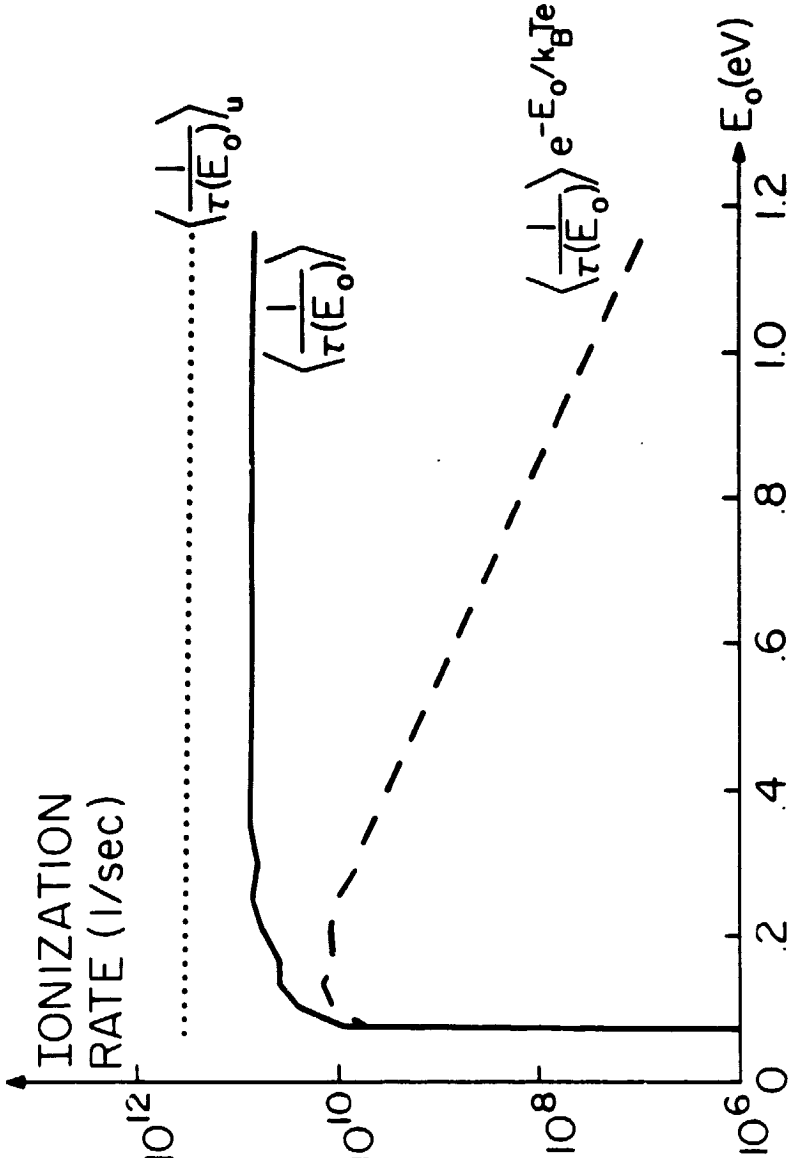

Figure 3. Same as Figure 4 except that $N_D = 1.0 \times 10^{18}$ cm^{-3}.

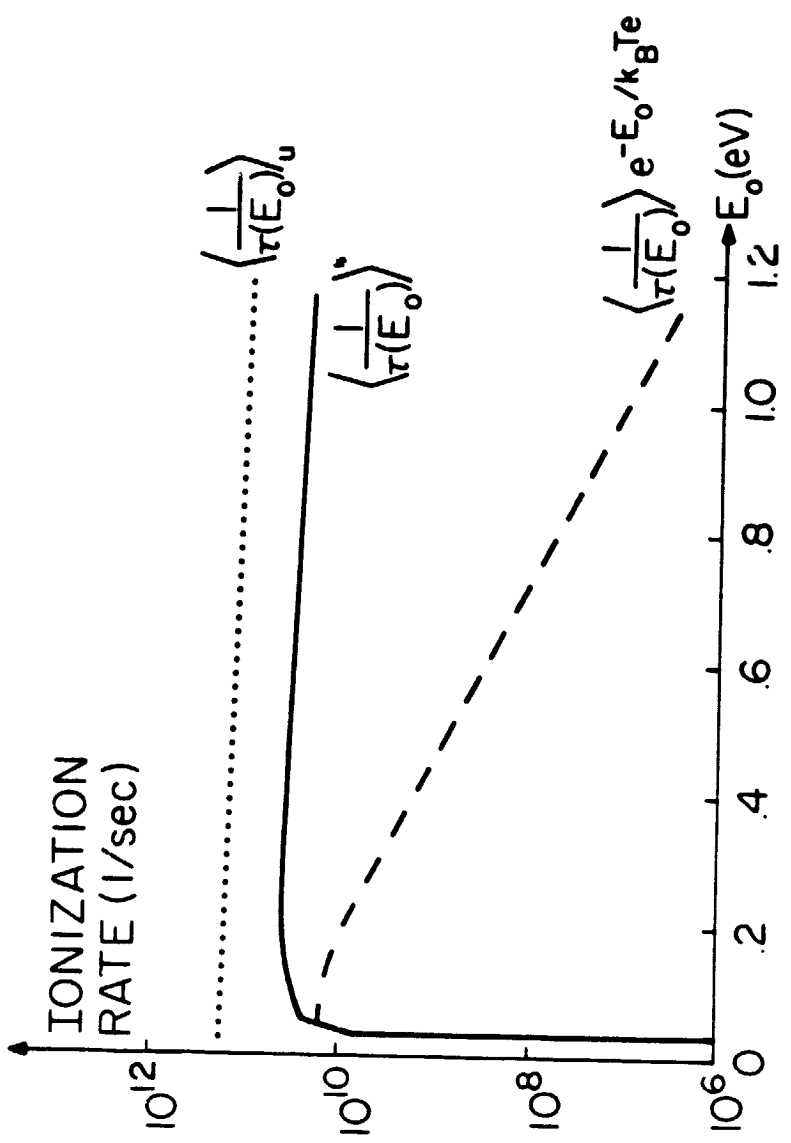

Figure 4. Same as Figure 4 except the L_z = 360Å.

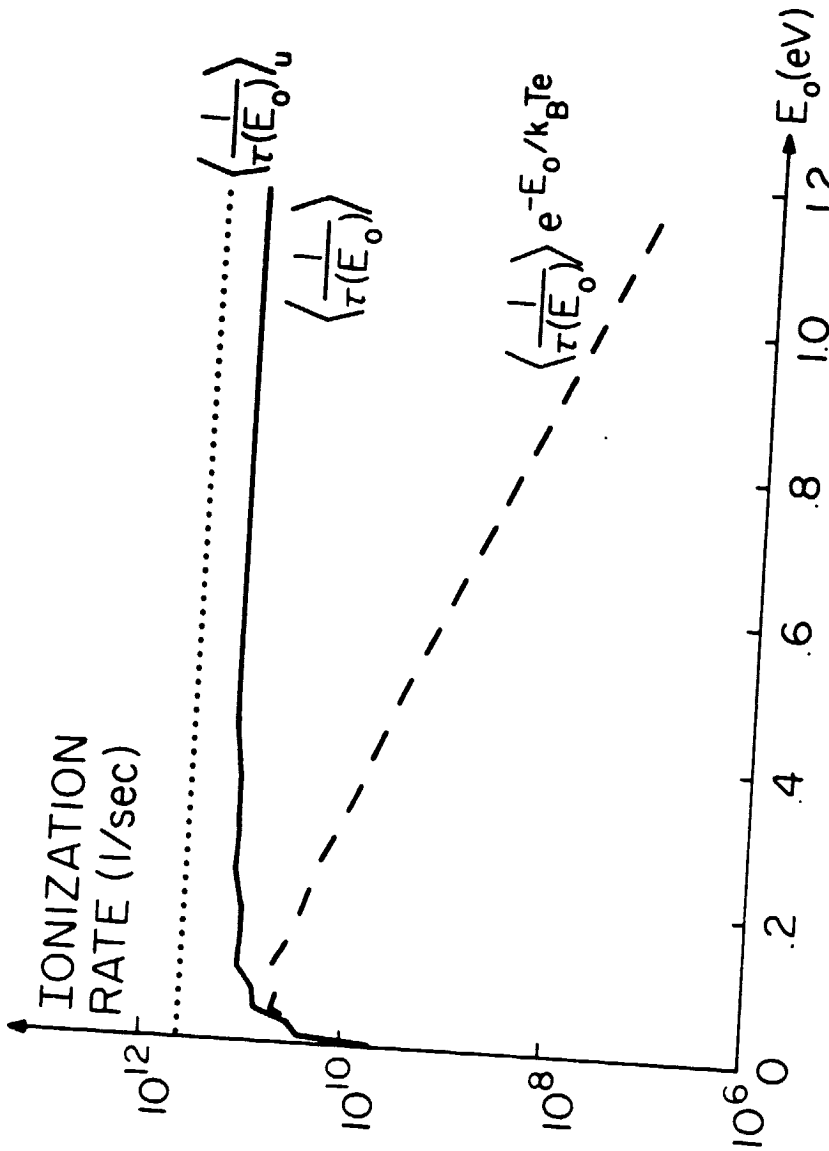

Figure 5. Same as Figure 4, except that $N_D = 1.0 \times 10^{18}$ cm^{-3} and $x = 0.20$.

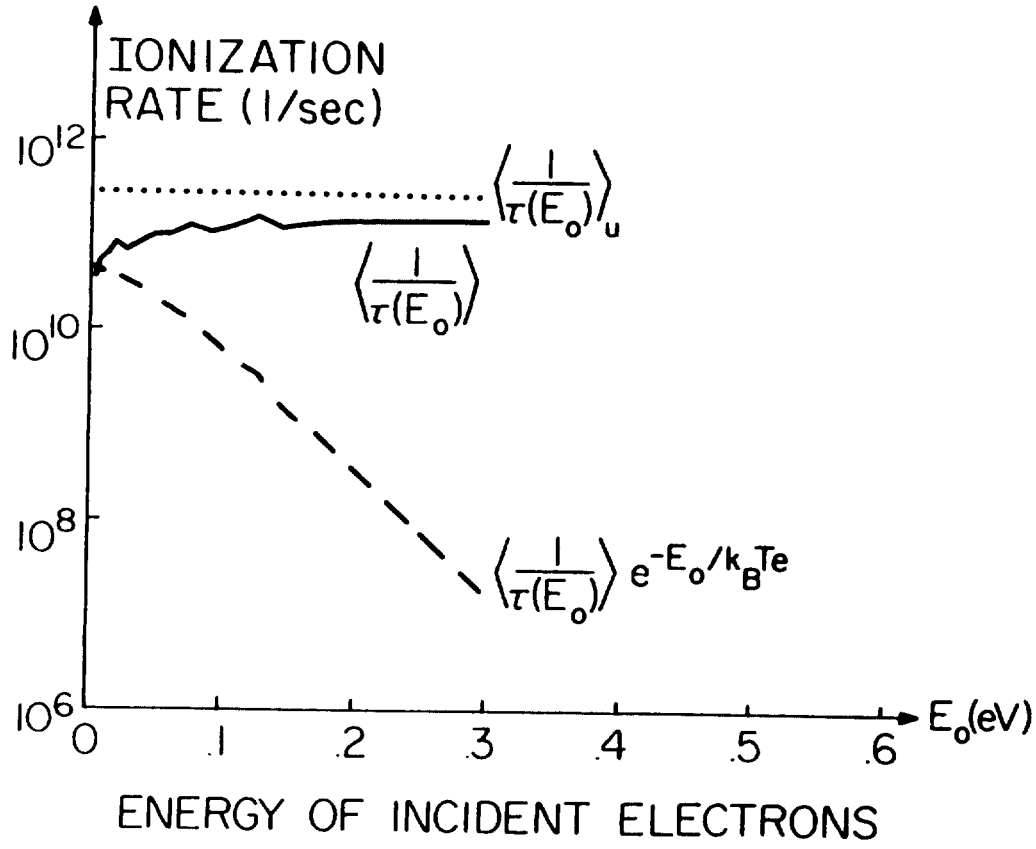

Figure 6. The impact ionization rate $\langle \frac{1}{\tau(E_0)} \rangle$ as a function of the incident hot electron energy E_0 ———— solid curve. $\langle \frac{1}{\tau(E_0)} \rangle \exp(-E_0/k_BT_e)$ ------ dashed curve. The upper limit of $\langle \frac{1}{\tau(E_0)} \rangle$ . . . . . dotted curve. $N_D = 1.0 \times 10^{18}$ cm^{-3}, $x = 0.2$, $L_z = 360$Å, $L = 1200$Å, $T = 77$°K, $T_e = 385$°K, $m^* \simeq 0.063\ m_0$, $m_0^* \simeq 0.0825\ m_0$.

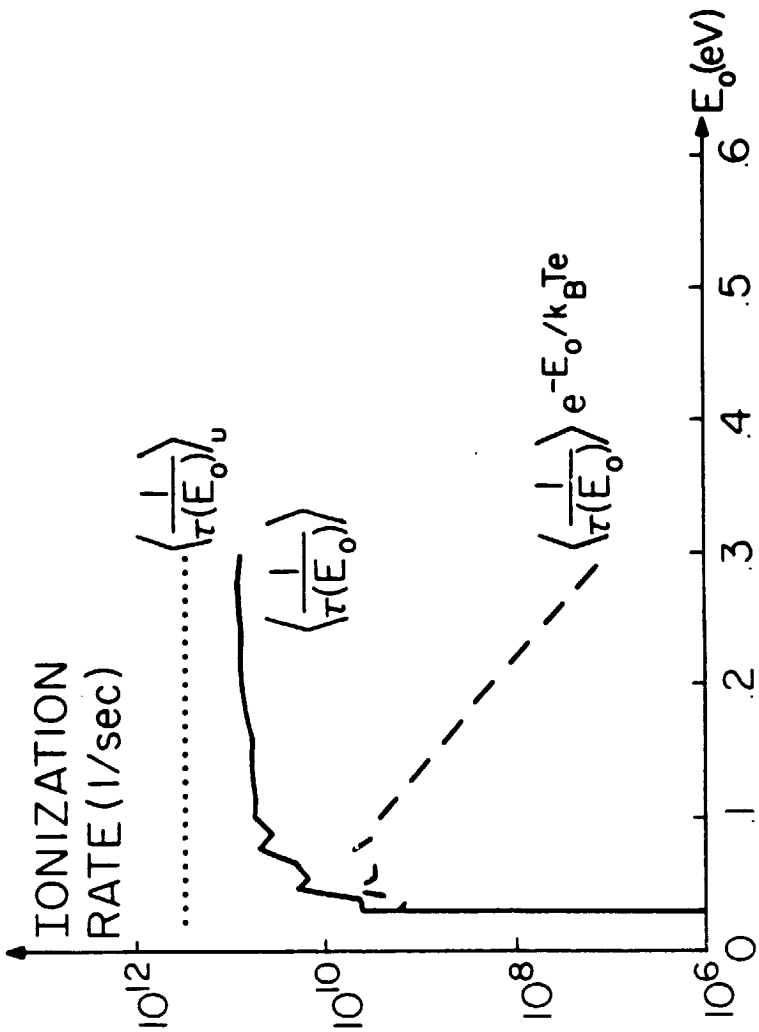

Figure 7. Same as Figure 8, except that x = 0.25.

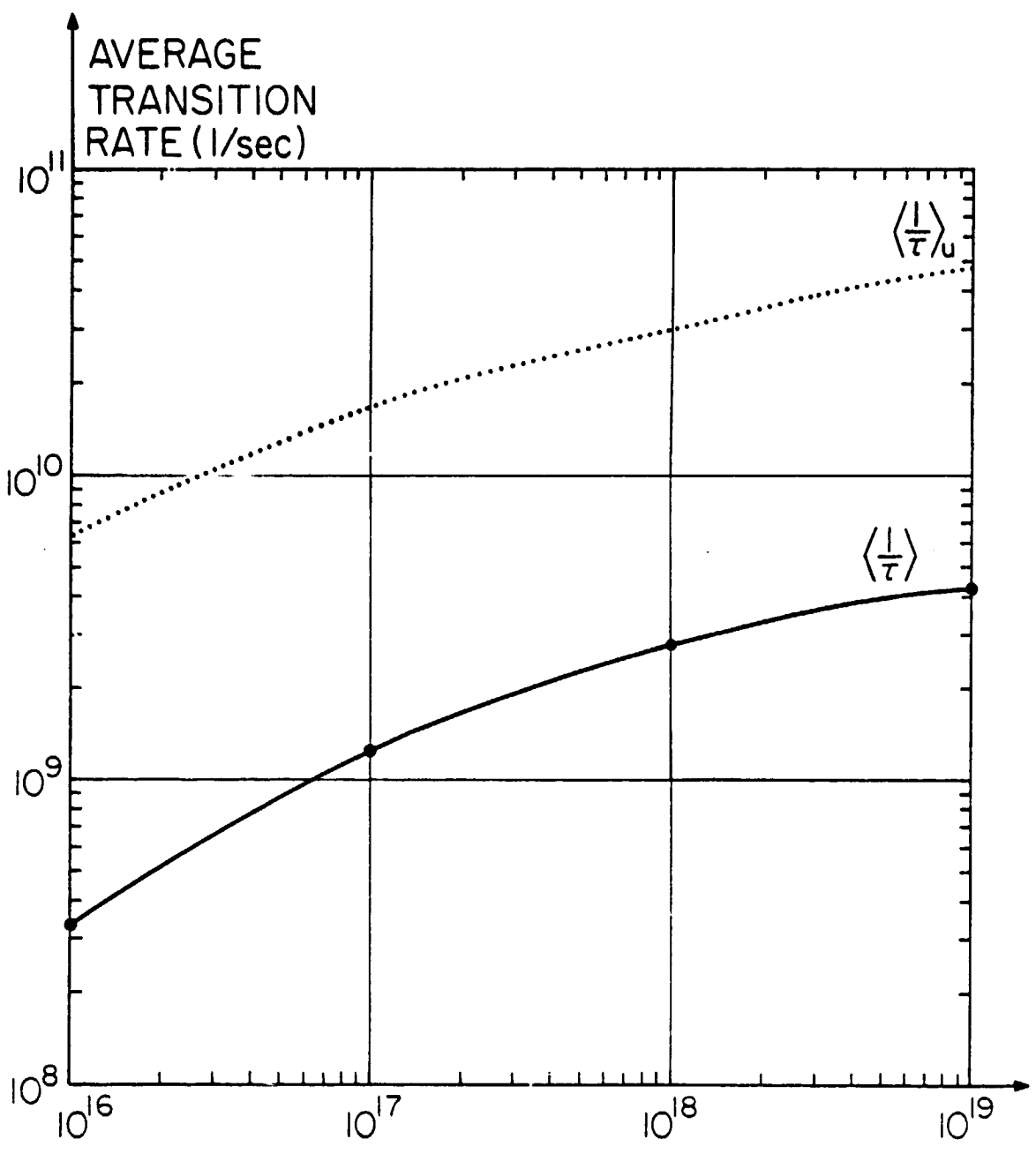

Figure 8. The total average ionization rate $\langle \frac{1}{\tau} \rangle$ as a function of the doping concentration N_D ——— solid curve. The upper limit, $\langle \frac{1}{\tau} \rangle_u$, is also given as the dotted curve.

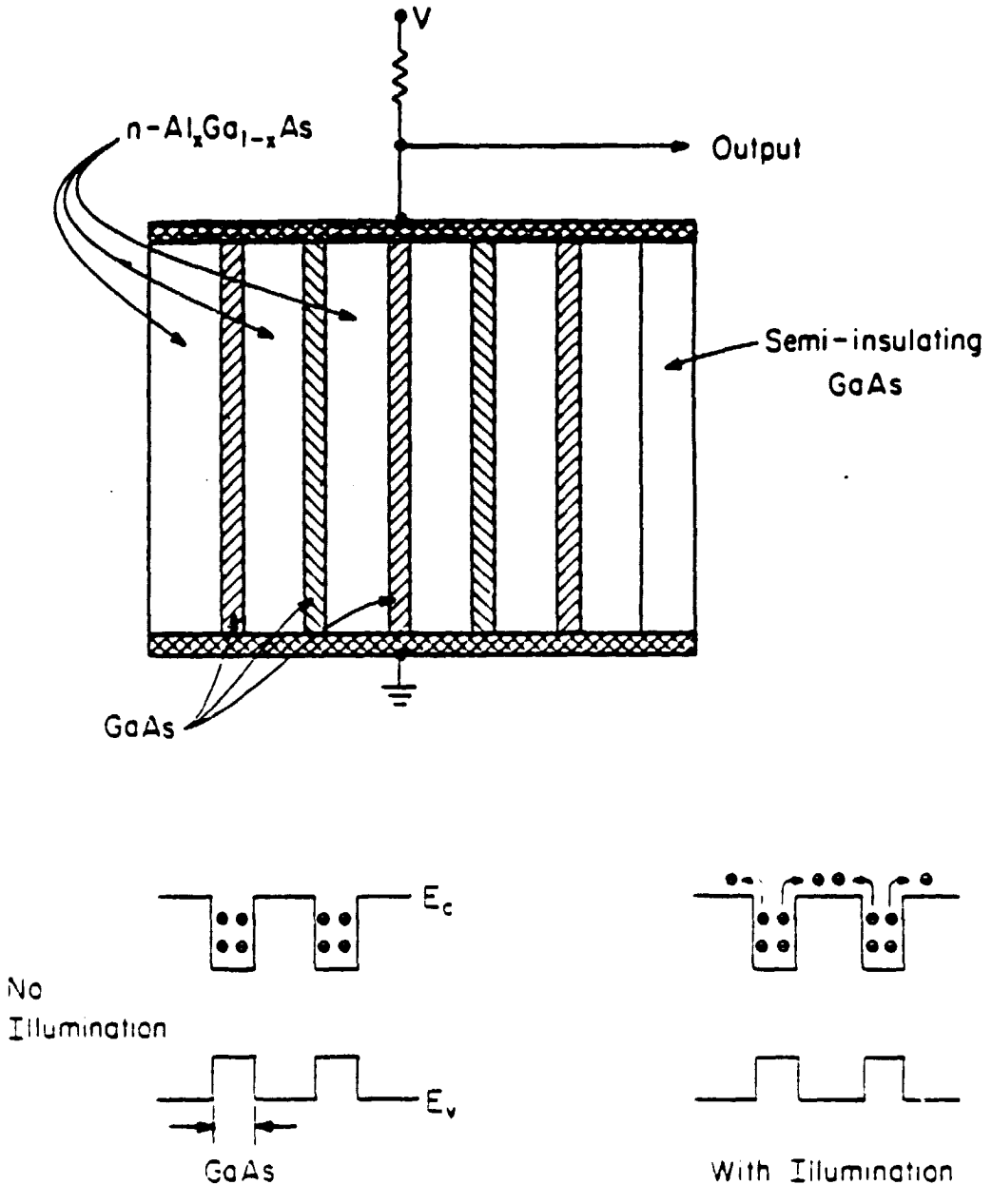

Figure 9. (a) Photodetectors using real space transfer mechanism.
(b) When no light is injected, electrons conduct in GaAs layers, where their mobility is large.
(c) With light injection, electrons conduct in $Al_xGa_{1-x}As$ layers, where their mobility is small.

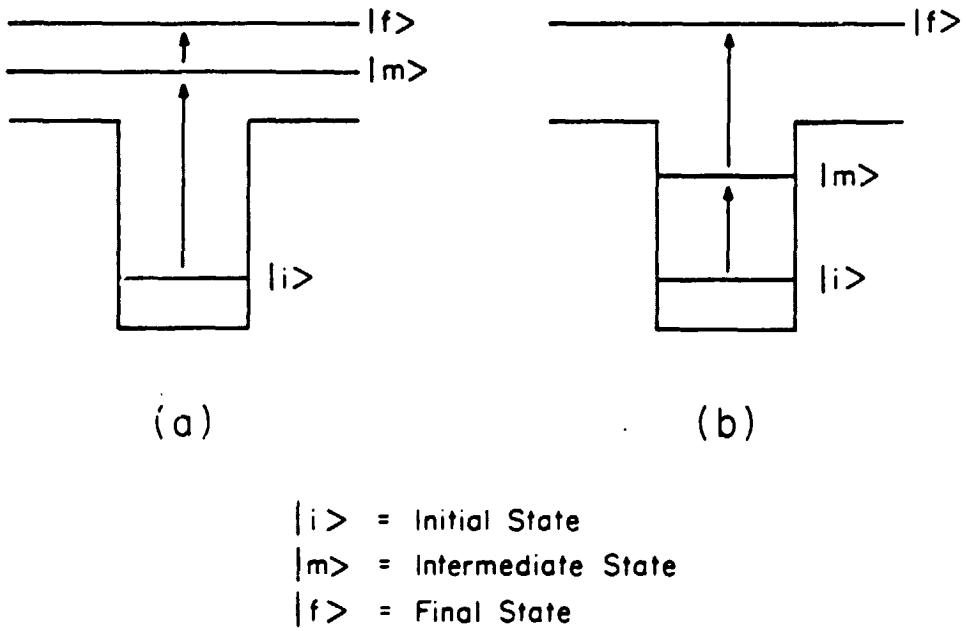

Figure 10. (a) Transition involving intermediate free state.
(b) Transition involving intermediate bound state.